Biophysical Chemistry 159 (2011) 110–119

Contents lists available at ScienceDirect

Biophysical Chemistry

journal homepage: http://www.elsevier.com/locate/biophyschem

# Heightened stability of polcalcin Phl p 7 is correlated with strategic placement of apolar residues

Michael T. Henzl *, Mark A. Reed, Anmin Tan

*Department of Biochemistry, University of Missouri, Columbia, MO 65211, United States*

ARTICLE INFO

*Article history:*
Received 28 March 2011
Received in revised form 18 May 2011
Accepted 18 May 2011
Available online 26 May 2011

*Keywords:*
$Ca^{2+}$-binding protein
EF-hand protein
Calorimetry
Urea denaturation
Protein stability

ABSTRACT

Phl p 7 exhibits atypical conformational stability and a diminutive denaturational heat capacity increment, $\Delta C_p$. Because exposure of apolar surface largely dictates the magnitude of $\Delta C_p$, a depressed value could signify an unusually compact unfolded state. The volume of the denatured state ensemble (DSE) is evidently inversely correlated with mean hydrophobicity [Pace et al., *Protein Sci. 19* (2010) 929–943]. Interestingly, apolar residues replace more polar ones at four positions in Phl p 7. We herein examine the consequences of replacing those residues with the corresponding ones from Bra n 1, a related isoform. All four mutations – M4H, L21A, I60T, and C63A – destabilize Phl p 7. Our analysis suggests that the DSE of Phl p 7 is indeed highly compact and that the substitutions act by increasing its volume and solvent-accessibility. All four mutations increase the urea *m* value; L21A, I60T, and C63A also yield a perceptible increase in $\Delta C_p$.

© 2011 Elsevier B.V. All rights reserved.

Polcalcins are small $Ca^{2+}$-binding proteins produced in the anthers and pollen of flowering plants [1–4]. Enrichment at the tips of growing pollen tubes implies a role in the control of pollen-tube growth [5]. There is evidence that polcalcins undergo a $Ca^{2+}$-dependent conformational change [1,2,5–9], consistent with an explicit regulatory function. However, the biological target protein has not been identified. Polcalcins are potent plant allergens, their allergenicity is primarily associated with the $Ca^{2+}$-bound form of the protein [1,6,10].

The polcalcin primary structure includes a highly conserved core sequence and a short, variable-length N-terminal extension (Fig. 1). Sequences range in length from 77 to 84 residues. As the solution structure of $Ca^{2+}$-bound Bet v 4 [11] illustrates (Fig. 2A), the polcalcin fold includes five α-helices. Four are associated with two EF-hand motifs, while the C-terminal 12 residues likewise adopt a helical configuration. The putative target-peptide binding site (Fig. 2B) is formed by helices α3 and α5 and select apolar side-chains from α2 and α4. Although the solution structure of $Ca^{2+}$-bound Phl p 7 has not been reported, the protein has been crystallized at low pH. However, under these conditions, the protein forms an unusual domain-swapped dimer [12]. Given that the protein is exclusively monomeric at neutral pH, the relevance of the dimeric crystal structure is uncertain.

The EF-hand is the defining structural element of the largest family of intracellular $Ca^{2+}$-binding proteins. The 30-residue motif consists of a 12-residue metal ion-binding loop flanked by short amphipathic helices [13–15]. The "EF-hand" moniker was bestowed by Kretsinger, who recognized that the helix–loop–helix arrangement could be mimicked with the fingers of the right hand [16]. Within the binding loop, the ligands to the bound metal ion are positioned at the vertices of an octahedron and indexed by Cartesian axes [17].

We recently examined the divalent ion-binding behavior of four polcalcin isoforms — Phl p 7, Bra n 1, Bra n 2, and Bet v 4 [8]. At 77 residues, Phl p 7 is the shortest of the four. Relative to Phl p 7, the other three proteins have N-terminal extensions of 1, 5, and 7 residues, respectively. Besides being the shortest of the four proteins, Phl p 7 displays an interesting sequence substitution in the binding loop of EF-hand 2. Aspartate replaces S55 at the $-x$ coordination position, a modification that confers heightened divalent ion affinity in the parvalbumin background.

Addition of the $Ca^{2+}$-bound proteins, but not the $Ca^{2+}$-free proteins, to a solution of ANS yields a substantial increase in fluorescence emission, implying that $Ca^{2+}$ binding provokes exposure of apolar surface. Consistent with that observation, all four proteins bind $Ca^{2+}$ with positive cooperativity. By contrast, addition of the polcalcins to ANS in the presence of $Mg^{2+}$ has no impact on the dye emission, and $Mg^{2+}$ binding is correspondingly noncooperative. Although the binding enthalpies associated with the first and second binding events differ significantly among the four proteins, the overall standard free energies for $Ca^{2+}$-binding fall in a fairly narrow range from $-17.3$ to $-18.2$ kcal $mol^{-1}$.

During our survey of polcalcin divalent ion-binding properties, we noted that Phl p 7 is substantially more stable than the other three isoforms. In phosphate-buffered saline, at pH 7.4, the apo-forms of Bet v 4, Bra n 1, Bra n 2, and Phl p 7 denature at 56.1, 57.9, 56.8, and

* Corresponding author at: Department of Biochemistry, 117 Schweitzer Hall, University of Missouri, Columbia, MO 65211, United States. Tel.: +1 573 882 7485; fax: +1 573 884 4812.
*E-mail address:* henzlm@missouri.edu (M.T. Henzl).

0301-4622/$ – see front matter © 2011 Elsevier B.V. All rights reserved.
doi:10.1016/j.bpc.2011.05.015

```
                    1                   10                  20                  30
Phl p 7             A D D M E R I F K R F D T N G D G K I S L S E L T D A L R T L G S T S
Bra n 1           A D A E H E R I F K K F D T D G D G K I S A A E L E E A L K K L G S V T
Bra n 2       A D A T E K A E H D R I F K K F D A N G D G K I S A S E L G D A L K N L G S V T
Bet v 4     A D D H P Q D K A E R E R I F K R F D A N G D G K I S A A E L G E A L K T L G S I T
                                          +x  +y  +z  -y  -x      -z

                    40                  50                  60                  70
Phl p 7     A D E V Q R M M A E I D T D G D G F I D F N E F I S F C N A N P G L M K D V A K V F
Bra n 1     P D D V T R M M A K I D T D G D G F I S F Q E F T E F A S A N P G L M K D V A K V F
Bra n 2     H D D I K R M M A E I D T D G D G Y I S Y Q E F S D F A S A N R G L M K D V A K I F
Bet v 4     P D E V K H M M A E I D T D G D G F I S F Q E F T D F G R A N R G L L K D V A K I F
                                  +x  +y  +z  -y  -x      -z
```

**Fig. 1.** Polcalcin amino acid sequences. The residue numbering scheme is based on Phl p 7, the shortest of the four proteins. The coordinating residues in the EF-hands are displayed in bold-face type, and the positions that they occupy in the binding loop are indicated below by the axes of a Cartesian coordinate system.

78.0 °C, respectively. Interestingly, unfolding of Phl p 7 is accompanied by a decidedly smaller change in heat capacity. Whereas Phl p 7 exhibits a $\Delta C_p$ of 0.34 kcal mol$^{-1}$ K$^{-1}$, the other three polcalcins display values of 0.66, 0.95, and 0.95 kcal mol$^{-1}$ K$^{-1}$, respectively.

There is increasing recognition that the random coil does not satisfactorily describe the denatured state for many proteins. The diminutive $\Delta C_p$ value suggested that Phl p 7 might adopt a relatively compact denatured state. Pace has suggested that the volume of the unfolded state is inversely correlated with hydrophobic content [18]. Inspection of the Bra n 1, Bra n 2, Bet v 4, and Phl p 7 sequences revealed four positions at which Phl p 7 harbors a more apolar side-chain — residues 4, 21, 60, and 63. It occurred to us that a detailed thermodynamic investigation of these sequence substitutions might be appropriate for inclusion in this special issue of Biophysical Chemistry dedicated to the first 25 years of the Gibbs Conference. Accordingly, we prepared single-site variants in which the Phl p 7 residue has been replaced with the corresponding residue from Bra n 1 — i.e., M4H, L21A, I60T, and C63A. We have also prepared the L21A/I60T, L21A/I60T/C63A, and M4H/L21A/I60T/C63A variants. The stability of each protein was evaluated by global analysis of DSC and urea-denaturation data. Our results suggest that Phl p 7 might provide a useful system for investigating the determinants of a compact denatured state.

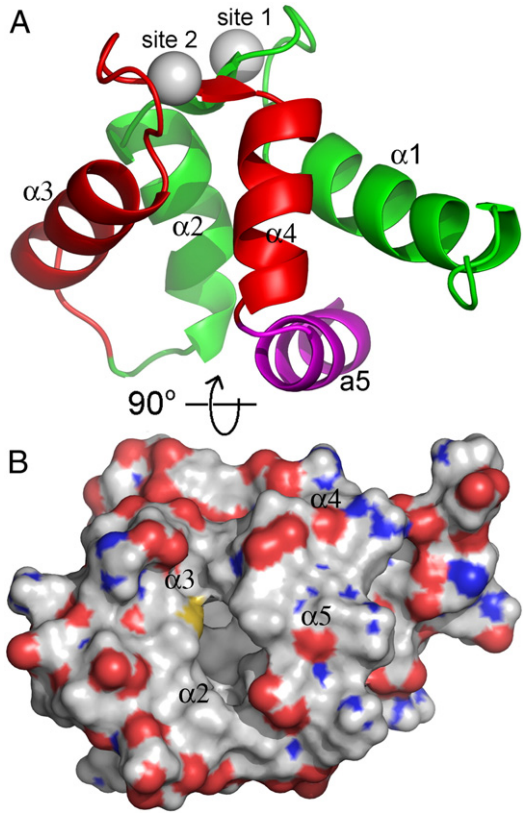


**Fig. 2.** Solution structure of $Ca^{2+}$-bound Bet v 4. (A) Ribbon diagram. EF-hand 1 (green) includes helices α1 and α2; EF-hand 2 (red) includes helices α3 and α4. Helix α5 (magenta), unique to the polcalcins consists of the final 12 residues. (B) Surface rendering, with anionic atoms colored red, neutral atoms colored gray/white, and cationic atoms colored blue. Orientation represents a 90° rotation of view (A). Coordinates are from PDB 1H4B [11].

## 1. Materials and methods

### 1.1. Materials

NaCl, 4-(2-hydroxyethyl)-1-piperazineethanesulfonic acid (Hepes), $CaCl_2 \cdot 2H_2O$, $\cdot MgCl_2 \cdot 2H_2O$, $\cdot NaH_2PO_4$, ethylene glycol-bis(2-aminoethylether)-*N*,*N*,*N*′,*N*′-tetraacetic acid (EGTA), nitrilotriacetic acid (NTA), ethylenediaminetetraacetic acid (EDTA), and Spectrapor 1 dialysis tubing (MWCO 6000–8000) were purchased from Fisher Scientific Co. High-purity urea (Fluka), dimyristoylphosphatidylcholine (DMPC), dipalmitoylphosphatidylcholine (DPPC), and distearoylphosphatidylcholine (DSPC) were obtained from Sigma-Aldrich Co.

### 1.2. Protein expression and purification

The Phl p 7 coding sequence, optimized for expression in *Escherichia. coli*, was synthesized by GenScript Corporation (Piscataway, NJ) and inserted into pET11a (Novagen), employing the Nde I and Bam HI restriction sites. The single M4H, L21A, I60T, and C63A mutations were introduced with the QuikChange® site-directed mutagenesis kit (Agilent), employing oligonucleotide primers from Integrated DNA Technologies, Inc. (Coralville, IA). Subsequently, I60 was mutated to threonine in the L21A background. Next, the C63A mutation was introduced in the 21/60 construct. This mutation necessitated the design of primers that harbored both the I60T and C63A mutations. Finally, M4 was replaced by histidine in the 21/60/63 background. In each case, the fidelity of the modified coding sequence was confirmed by automated DNA sequencing. The protocols employed for expression and purification of the variant proteins were identical to those described previously [8]. Protein concentrations were estimated spectrophotometrically, employing a molar extinction coefficient at 257 nm of 1400 M$^{-1}$ cm$^{-1}$.

### 1.3. Isothermal titration calorimetry (ITC)

Residual $Ca^{2+}$ was removed from the protein preparations prior to analysis by treatment with EDTA-derivatized agarose [19,20], as described previously [8]. The resulting material contained less than 0.02 molar equivalents of $Ca^{2+}$ by atomic absorption. Similarly treated buffer contained undetectable levels of $Ca^{2+}$ (<0.2 μM).

ITC experiments were conducted at 25 °C and pH 7.4 in Hepes-buffered saline, using a VP-ITC calorimeter (MicroCal, LLC). Following thermal equilibration, titrant was added to the 1.41 mL sample at 240-sec intervals. All titrations included a 2 μL pre-addition, the heat from which was neglected during data analysis. The $Ca^{2+}$ titrant was standardized by titrating an EDTA solution, prepared from analytical reagent-grade $Na_2EDTA \cdot 2H_2O$.

Samples of protein (typically 50–60 μM) were titrated with $Ca^{2+}$ in the presence and absence of competitive chelators (EDTA, EGTA, and NTA). The raw data were integrated using software supplied with the instrument and compiled into a single dataset. The composite dataset was then subjected to simultaneous least-squares minimization, to obtain estimates of the $Ca^{2+}$-binding constants and -enthalpies consistent with all of the titrations [21]. After identifying the optimal parameter values and the lowest chi-square, $\chi^2(min)$, confidence intervals were estimated as described elsewhere [8,22].

The polcalcins bind $Ca^{2+}$ with positive cooperativity, necessitating the use of macroscopic binding constants. The cumulative heat of binding after titrant addition $i$ is expressed by

$$Q_i = 10^6 \cdot V \cdot P_T \left( \frac{\Delta H_1 K_1 \left[Ca^{2+}\right] + (\Delta H_1 + \Delta H_2) K_2 K_1 \left[Ca^{2+}\right]^2}{1 + K_1 \left[Ca^{2+}\right] + K_2 K_1 \left[Ca^{2+}\right]^2} \right) \quad (1)$$

where $V$ is the sample volume, $P_t$ the total protein concentration, $\Delta H_1$ and $\Delta H_2$ the binding enthalpies for the first and second binding events, and $K_1$ and $K_2$ the first and second stepwise binding constants. In competitive titrations, a term for binding of $Ca^{2+}$ by the chelator is included

$$Q_i = 10^6 \cdot V \cdot \left[ P_T \left( \frac{\Delta H_1 K_1 \left[Ca^{2+}\right] + (\Delta H_1 + \Delta H_2) K_2 K_1 \left[Ca^{2+}\right]^2}{1 + K_1 \left[Ca^{2+}\right] + K_2 K_1 \left[Ca^{2+}\right]^2} \right) + I_t \frac{\Delta H_I K_I \left[Ca^{2+}\right]}{1 + K_I \left[Ca^{2+}\right]} \right]. \quad (2)$$

In this equation, $I_t$ represents the total chelator concentration, and $\Delta H_I$ and $K_I$ are the binding enthalpy and association constant for the $Ca^{2+}$-chelator complex.

The injection heats are modeled as the difference between the cumulative heats associated with injections $i$ and $i-1$:

$$q_i = (Q_i - Q_{i-1}) + \left(\frac{dV_i}{V}\right)\left(\frac{Q_i + Q_{i-1}}{2}\right). \quad (3)$$

The latter term in Eq. (3) corrects for the heat associated with the volume of solution displaced from the sample cell by the $i^{th}$ titrant addition, where $dV_i$ is the volume of that injection. A more detailed discussion of the least-squares analysis and estimation of parameter uncertainties is presented elsewhere [8].

### 1.4. Chemical denaturation

Samples (2.0 mL, 5.0 μM) of $Ca^{2+}$-free protein, in phosphate-buffered saline (PBS) containing 0.5 mM EDTA, were titrated with urea while monitoring ellipticity at 222 nm in an Aviv 62DS circular dichroism spectrometer. Aliquots of denaturant were added with an automated titrator (Hamilton Microlab 500), operated in constant-volume mode. Following each injection, the sample was allowed to equilibrate with stirring for 120 s prior to data acquisition (30 s). Control experiments confirmed that unfolding was complete on this time scale.

To prepare the 10.0 M titrant solution, 60.07 g of urea was transferred to a 100 mL volumetric flask, with 10.0 mL of a 10× PBS solution. After adding sufficient water to dissolve the urea and equilibration to room temperature, the volume was adjusted to 100.0 mL, and the pH was readjusted to 7.40. The actual urea concentration was estimated with a refractometer, using the relationship $M = 117.66(\Delta\eta) + 29.753(\Delta\eta)^2 + 185.56(\Delta\eta)^3$ [23] where $\Delta\eta$ represents the refractive index difference between the urea solution and buffer. The calculated and measured concentrations agreed within 1%.

### 1.5. Differential scanning calorimetry (DSC)

DSC was performed in a Nano-DSC (Calorimetry Sciences Corporation), equipped with cylindrical hastalloy cells. Temperature calibration was verified with DMPC, DPPC, and DSPC, and the accuracy of the differential power measurements was verified with internally generated electrical calibration pulses.

Samples were dialyzed extensively against PBS containing 0.005 M EDTA, pH 7.4, which then served as the reference. Sample and reference solutions were briefly degassed under vacuum prior to loading. A scan rate of 60°/h was employed for all experiments. All of the proteins included in the study exhibit an endotherm on rescan, comparable in magnitude to the original, indicating reversible denaturation. A baseline, obtained with sample- and reference cells filled with buffer, was subtracted from the protein data prior to analysis. Heat capacity data collected at four protein concentrations were subjected to global nonlinear least-squares analysis to extract estimates of the melting temperature ($T_m$), van't Hoff enthalpy ($\Delta H_{vH}$), calorimetric enthalpy ($\Delta H_{cal}$), and denaturational heat capacity increment ($\Delta C_p$), using the two-state unfolding model described by Haynie [24].

To improve the $\Delta C_p$ estimates, we supplemented the DSC data with urea denaturation data, as suggested by Pace and Laurents [25]. Samples (5.0 μM) were titrated with urea at several temperatures, and the resulting ellipticity data, collected at 222 nm, were analyzed simultaneously with the DSC data. The global analysis is patterned after McCrary et al. [26]. The following equation for a two-state unfolding transition [27] was used to treat the chemical denaturation data:

$$y = \frac{(y_n + m_n[urea]) + (y_u + m_u[urea]) * \exp(-(\Delta G_o - m[urea])/RT)}{1 + \exp(-(\Delta G_o - m[urea])/RT)} \quad (4)$$

where $\Delta G_o$ is the conformational stability in the absence of urea, $m$ is the sensitivity of the protein to the denaturant concentration, $y_n$ and $m_n$ are the intercept and slope of the pre-transition baseline, and $y_u$ and $m_u$ are the corresponding values for post-transition baseline. Instead of treating $\Delta G_o$ as a fitting parameter, however, its value was calculated using the Gibbs–Helmholtz equation:

$$\Delta G_o = \Delta H_{vH}\left(1 - \frac{T}{T_m}\right) + \Delta C_p[(T - T_m) - T\ln(T/T_m)]. \quad (5)$$

Thus, least-squares minimization selects for values of $T_m$, $\Delta H_{vH}$, $\Delta C_p$, and $m$ that are consistent with both the chemical and thermal denaturation data. Each protein was titrated with urea at four temperatures, spaced at five-degree intervals. The temperature range employed for each analysis was determined by the stability of the protein under consideration. Parameter uncertainties were evaluated by confidence-interval analysis.

## 2. Results

### 2.1. $Ca^{2+}$-binding behavior

Fig. 3 displays raw ITC data for Phl p 7 and each of the variant proteins characterized in this study. Because the experiments

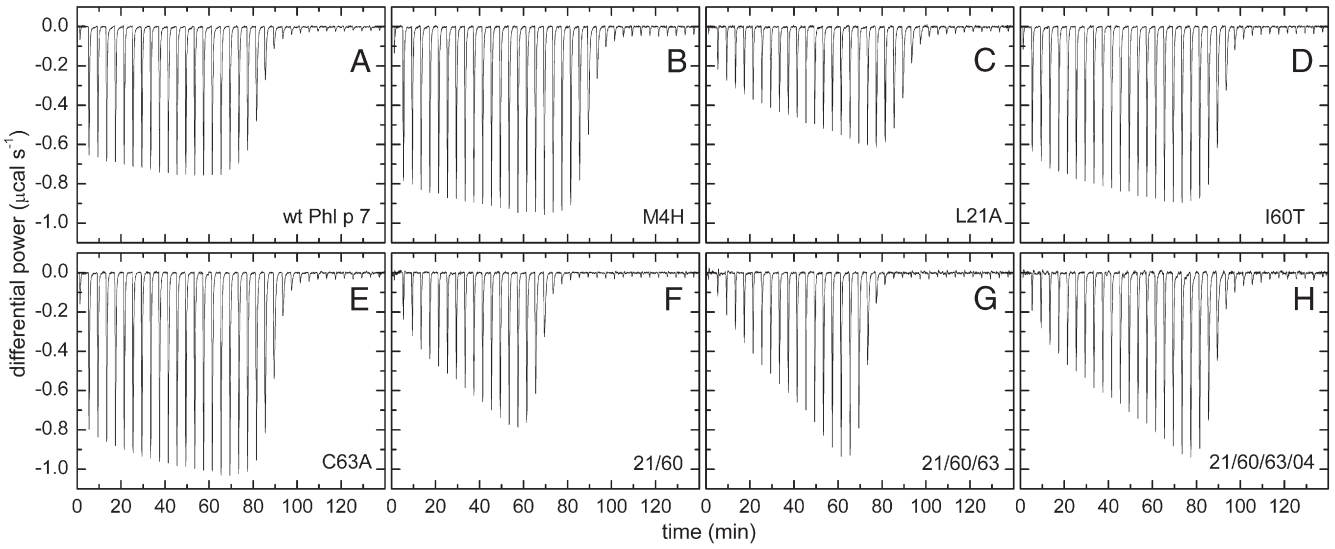


**Fig. 3.** Raw ITC data. Phl p 7 and the seven site-specific variant proteins were titrated with $Ca^{2+}$, yielding the raw data displayed above. The titrant concentration was 1.1 mM in each case, and all injection volumes were 7.0 μL, excepting the initial 2 μL pre-injection. Protein concentrations ranged from 60 to 70 μM.

employed identical titrant concentrations and injection volumes, the data sets have been plotted on the same vertical scale, to facilitate comparison. Clearly, the mutations impact both the magnitude and overall pattern of the injection heats. Given that the $Ca^{2+}$ coordination geometry should be unchanged by the mutations, the variant proteins could logically be expected to possess identical intrinsic $Ca^{2+}$-binding enthalpies. There is, however, strong spectroscopic evidence that $Ca^{2+}$ binding provokes a major structural alteration in the polcalcin molecule. Thus, the observed binding heat represents the sum of the $Ca^{2+}$-binding enthalpies per se plus the enthalpy associated with the attendant conformational change. Apparently, the sequence substitutions impact the energetics of the latter.

As described in Materials and methods, the proteins were also titrated with $Ca^{2+}$ in the presence of several metal ion chelators (EDTA, EGTA, and NTA). The data collected with and without chelators present were subjected to simultaneous least-squares minimization, to obtain estimates for the binding constants and enthalpies. The data were treated with a two-site Adair model (Eqs. (1) and (2)). Integrated data and optimal fits are presented in Figs. 4 and 5 for two representative analyses, the L21A and M4H variants. Parameter values and associated uncertainties for each of the proteins are listed in Table 1, along with the calculated overall standard free energy for $Ca^{2+}$ binding.

With the exception of the L21A substitution, the single mutations yield a perceptible increase in $Ca^{2+}$ affinity. Although the isolated L21A mutation slightly lowers $Ca^{2+}$ affinity, when combined with I60T, the resulting protein exhibits a significant increase in $Ca^{2+}$ affinity, relative to the wild-type protein. The introduction of C63A into the 21/60 double variant has no perceptible impact on overall $Ca^{2+}$ affinity. However, introduction of M4H into the triple variant reduces overall affinity by 0.30 kcal mol$^{-1}$.

$Ca^{2+}$ binding becomes enthalpically less favorable upon replacement of L21 with alanine. In the wild-type protein, the mutation yields a $\Delta\Delta H$ of 2.07 kcal mol$^{-1}$. In the context of I60T, introduction of L21A produces a $\Delta\Delta H$ of 2.09 kcal mol$^{-1}$. By contrast, the other three isolated mutations improve the overall enthalpy of $Ca^{2+}$ binding. The enthalpic impact of I60T is comparable whether introduced into the wild-type protein ($\Delta\Delta H = -0.69$ kcal mol$^{-1}$) or into L21A ($\Delta\Delta H = -0.77$ kcal mol$^{-1}$). Likewise, the impact of M4H in the 21/60/63 variant ($\Delta\Delta H = -0.87$) is qualitatively similar to its effect in wild-type Phl p 7 ($\Delta\Delta H = -1.24$ kcal mol$^{-1}$). By contrast, whereas $Ca^{2+}$ binding becomes enthalpically more favorable when C63 is replaced by alanine in the wild-type protein ($\Delta\Delta H = -1.85$ kcal mol$^{-1}$), introduction of C63A into the 21/60 variant affords a $\Delta\Delta H$ of $+0.12$ kcal mol$^{-1}$.

### 2.2. Conformational stability

The conformational stabilities of the various proteins were examined by global analysis of thermal and chemical-denaturation data. Extraction of reliable $\Delta C_p$ values from single DSC analyses can be problematic, due to baseline irreproducibility. Therefore, DSC data

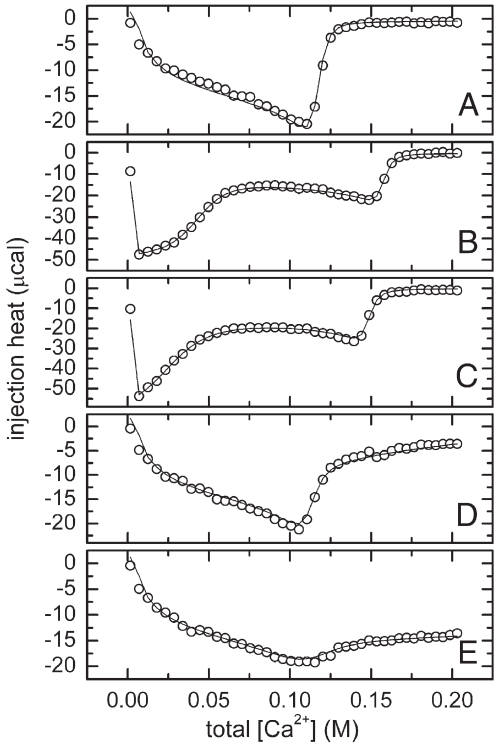


**Fig. 4.** L21A $Ca^{2+}$-binding behavior. The titrant concentration was 1.1 mM, and all injection volumes were 7.0 μL. (A) 63 μM L21A. (B) 57 μM L21A, 55 μM EDTA. (C) 57 μM L21A, 45 μM EGTA. (D) 55 μM L21A, 100 μM NTA. (E) 55 μM L21A, 1.0 mM NTA.

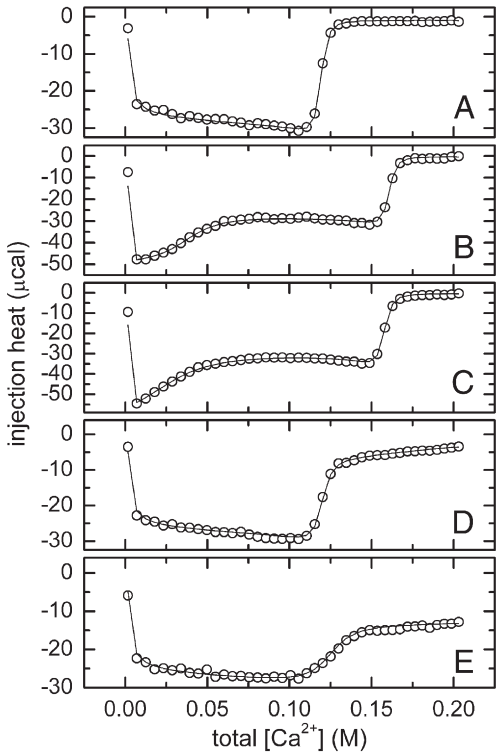


**Fig. 5.** M4H $Ca^{2+}$-binding behavior. The titrant concentration was 1.1 mM, and all injection volumes were 7.0 μL. (A) 64 μM M4H. (B) 67 μM M4H, 50 μM EDTA. (C) 64 μM M4H, 50 μM EGTA. (D) 64 μM M4H, 100 μM NTA. (E) 64 μM M4H, 1.0 mM NTA.

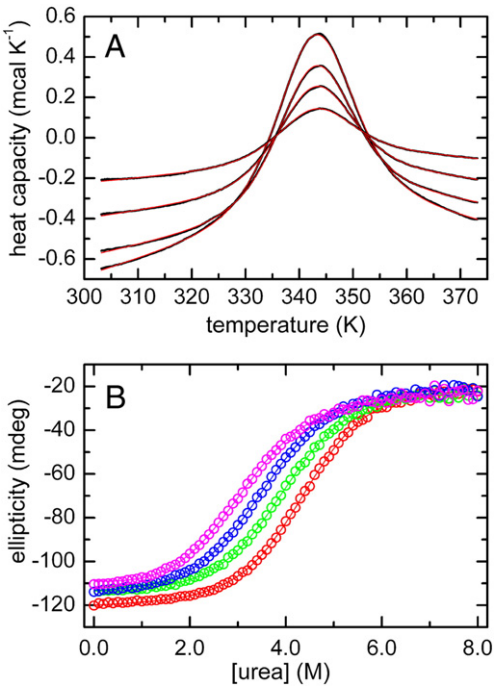


**Fig. 6.** Global analysis of L21A conformational stability. Samples of the protein were subjected to scanning calorimetry and CD-monitored chemical denaturation. The resulting data were subjected to global least-squares minimization, as described in Materials and methods (A) DSC was performed on the L21A variant at concentrations of 2.1, 3.9, 5.7, and 6.9 mg/mL. The black lines depict the protein heat capacity data, following subtraction of the buffer contribution; the red lines indicate the optimal least-squares fit. (B) Urea denaturation. 5.0 μM samples of the protein were titrated with 10.0 M urea at 35 (red), 40 (green), 45 (blue), and 50 (magenta) °C. Ellipticity was monitored at 222 nm. The solid lines through the data points represent the best least-squares fit.

were collected at four protein concentrations and analyzed simultaneously with CD-monitored urea denaturation data collected at four different temperatures. Analysis of the resulting composite data set yielded estimates for the melting temperature, the van't Hoff and calorimetric enthalpies, and the heat capacity change upon unfolding.

Representative analyses are presented in Figs. 6 and 7, for L21A and the 21/60 double variant, respectively. The parameters obtained for each of the variant proteins are presented in Table 2, along with the values previously reported for Phl p 7 and Bra n 1. The calculated changes in the thermodynamic properties, evaluated at the wild-type Phl p 7 melting temperature (77.3 °C) and at 25 °C, are summarized in Table 3.

Of the four single mutations examined, L21A has the greatest impact on stability. Replacement of L21 by alanine lowers the $T_m$ by 8.2°, raises $\Delta C_p$ by 0.24 kcal $mol^{-1}$ $K^{-1}$, lowers the van't Hoff enthalpy ($\Delta H_{vH}$) by 1.2 kcal $mol^{-1}$ and the calorimetric enthalpy ($\Delta H_{cal}$) by 4.1 kcal $mol^{-1}$. Evaluated at the wild-type $T_m$, L21A lowers the stability at by 1.3 kcal $mol^{-1}$. The extrapolated decrease in stability at 25 °C is 1.6 kcal $mol^{-1}$.

I60T has the second largest effect on Phl p 7 stability, dropping the $T_m$ by 6.9° and raising $\Delta C_p$ by 0.17 kcal $mol^{-1}$ $K^{-1}$. The mutation raises $\Delta H_{vH}$ to 53.7 kcal $mol^{-1}$ and $\Delta H_{cal}$ to 63.1 kcal $mol^{-1}$. The resulting destabilization, evaluated at 77.3 °C, is 1.1 kcal $mol^{-1}$. The extrapolated $\Delta\Delta G$ value at 25 °C is −0.9 kcal $mol^{-1}$.

**Table 1**
$Ca^{2+}$-binding parameters.

| Protein | $K_1$[a] $M^{-1}$ | $\Delta H_1$ kcal/mol | $K_2$[a] $M^{-1}$ | $\Delta H_2$ kcal/mol | $\Delta G_{tot}$ kcal/mol |
|---|---|---|---|---|---|
| Phl p 7 | $1.90\times10^6$ | −1.96 | $6.44\times10^6$ | −3.95 | −17.8 |
| | (1.71, 2.09) | (−2.07, −1.85) | (5.72, 7.27) | (−4.07, −3.84) | (−18.0, −17.7) |
| M4H | $1.81\times10^6$ | −1.86 | $1.31\times10^7$ | −5.29 | −18.2 |
| | (1.68, 1.97) | (−1.91, −1.80) | (1.10, 1.43) | (−5.34, −5.24) | (−18.3, −18.1) |
| L21A | $1.52\times10^6$ | 1.35 | $7.09\times10^6$ | −5.19 | −17.7 |
| | (1.40, 1.62) | (1.28, 1.42) | (6.24, 8.16) | (−5.29, −5.08) | (−17.9, −17.6) |
| I60T | $2.07\times10^6$ | −0.56 | $1.54\times10^7$ | −5.94 | −18.4 |
| | (1.91, 2.24) | (−0.62, −0.51) | (1.34, 1.75) | (−6.00, −5.88) | (−18.5, −18.3,) |
| C63A | $2.25\times10^6$ | −1.34 | $1.53\times10^7$ | −6.42 | −18.4 |
| | (1.95, 2.53) | (−1.43, −1.26) | (1.28, 1.89) | (−6.29, −6.55) | (−18.6, −18.3) |
| L21A-I60T | $4.37\times10^6$ | 0.63 | $6.68\times10^6$ | −5.14 | −18.3 |
| | (3.98, 4.81) | (0.54, 0.75) | (5.74, 8.55) | (−5.24, −4.99) | (−18.6, −18.2) |
| 21-60-63 | $4.57\times10^6$ | 1.21 | $6.09\times10^6$ | −5.60 | −18.3 |
| | (4.16, 4.93) | (1.04, 1.33) | (5.34, 7.36) | (−5.71, −5.48) | (−18.5, −18.2) |
| 21-60-63-4 | $3.94\times10^6$ | 0.63 | $4.42\times10^6$ | −5.89 | −18.0 |
| | (3.39, 4.37) | (0.51, 0.78) | (3.71, 5.70) | (−6.06, −5.71) | (−18.3, −17.9) |

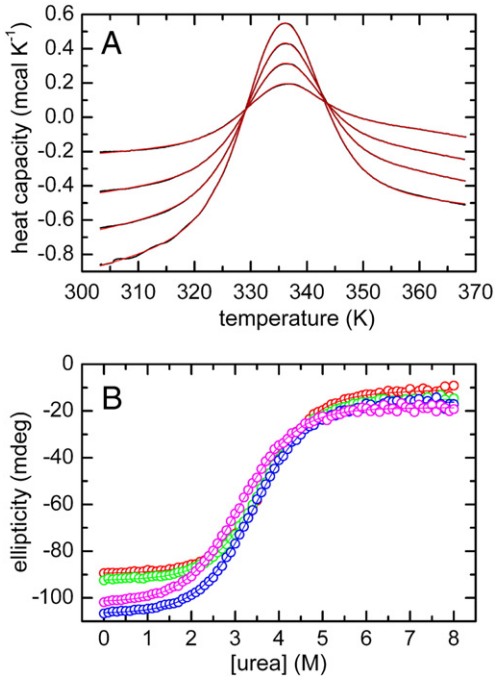


**Fig. 7.** Analysis of L21A/I60T conformational stability. (A) DSC data acquired at 8.6, 6.5, 4.3, and 2.2 mg/mL. Heat capacity data, after subtraction of the buffer blank, are shown in black; the red lines indicate the optimal fit. (B) Urea denaturation at 20 (red), 25 (green), 30 (blue), and 40 (magenta) °C. Solid lines through the ellipticity data (222 nm) represent the optimal least-squares fit.

Replacement of C63 with alanine lowers the $T_m$ by 2.8°, reduces $\Delta H_{vH}$ by 1.8 kcal mol$^{-1}$, leaves $\Delta H_{cal}$ essentially unchanged, and shifts $\Delta C_p$ upwards by 0.08 kcal mol$^{-1}$ K$^{-1}$. The decrease in stability at the wild-type $T_m$ is −0.4 kcal mol$^{-1}$. The extrapolated stability at 25 °C is reduced by 0.8 kcal mol$^{-1}$.

Replacement of M4 with histidine lowers the $T_m$ by 3.7°, reduces $\Delta H_{vH}$ by 3.6 kcal mol$^{-1}$, and reduces $\Delta H_{cal}$ by 4.1 kcal mol$^{-1}$. In contrast to the other three mutations, which all raise $\Delta C_p$, the isolated M4H mutation lowers $\Delta C_p$ by 0.03 kcal mol$^{-1}$. The extrapolated conformational stability of M4H is 0.5 kcal mol$^{-1}$ at the wild-type $T_m$ and 0.7 kcal mol$^{-1}$ lower at 25 °C.

The energetic consequences of the L21A and I60T mutations are approximately additive. The individual $T_m$ shifts are 8.2 and 6.9°, respectively, and the 21/60 double variant exhibits a $\Delta T_m$ of 16.0°. Likewise, L21A and I60T raise $\Delta C_p$ by 0.24 and 0.17 kcal mol$^{-1}$ K$^{-1}$, respectively, and the 21/60 variant exhibits a $\Delta\Delta C_p$ of 0.44 kcal mol$^{-1}$ K$^{-1}$. The extrapolated stability of 21/60 at 25 °C, at 3.8 kcal mol$^{-1}$, is 2.4 kcal mol$^{-1}$ lower than that of wild-type Phl p 7. This calculated reduction in stability very nearly equals the combined reductions observed for the single-site variants.

By contrast, the impact of the C63A mutation is context dependent. Whereas the isolated mutation lowers the $T_m$ by 2.8°, when introduced into 21/60, C63A lowers the $T_m$ by 3.5°. Whereas the isolated mutation lowers $\Delta H_{vH}$ by 1.8 kcal mol$^{-1}$, introduction of C63A into 21/60 lowers $\Delta H_{vH}$ by 3.6 kcal mol$^{-1}$. And whereas the isolated mutation raises $\Delta C_p$ by 0.08 kcal mol$^{-1}$ K$^{-1}$, in the context of 21/60, C63A lowers $\Delta C_p$ by 0.03 kcal mol$^{-1}$ K$^{-1}$. As a result, the mutation reduces the stability of 21/60 at 25 °C by 0.5 kcal/mol, as compared to 0.8 kcal mol$^{-1}$ in wild-type Phl p 7.

The impact of M4H is likewise context-dependent. In the presence of the other three mutations, the $\Delta T_m$ is just −2.8°, rather than −3.7; $\Delta\Delta H_{vH}$ is nearly zero, rather than −3.6 kcal/mol; and the $\Delta\Delta C_p$ value is 0.13 kcal mol$^{-1}$ K$^{-1}$, rather than −0.03 kcal mol$^{-1}$ K$^{-1}$. In the 21/60/63 background, M4H lowers the extrapolated stability of wild-type Phl p 7 at 25 °C by 0.7 kcal/mol, as compared to just 0.3 kcal/mol in the context of the wild-type protein.

In addition to perturbing $\Delta C_p$, the mutations also influence the *m* value, which describes the sensitivity of the protein stability to urea denaturation. However, the *m*-value alterations are more modest. Whereas wild-type Phl p 7 exhibits an *m*-value of 0.83 kcal mol$^{-1}$ M$^{-1}$, the 21/60/63/04 variant exhibits an *m*-value of just 1.15. Moreover, the variations in the *m*-value do not precisely parallel the changes in $\Delta C_p$. For example, M4H causes a small decrease in $\Delta C_p$ but increases *m* from 0.83 to 0.96 kcal mol$^{-1}$ M$^{-1}$. The *m*-value and $\Delta C_p$ are both thought to qualitatively reflect the solvent accessibility of the unfolded state. Clearly, however, the denatured state ensembles resulting from thermal and chemical denaturation will not be equivalent. In the latter, in addition to the solvent interactions with the polypeptide backbone and side-chains, the backbone interacts strongly with urea.

Fig. 8 displays the changes in unfolding energetics resulting from these mutations at 77.3 °C, the melting temperature of wild-type Phl p 7. The relatively minor reductions in stability produced by the isolated C63A and M4H mutations – 0.4 and 0.5 kcal mol$^{-1}$, respectively – are evidently achieved by lowering the enthalpy change required for unfolding. By contrast, the larger reductions in $\Delta G_{conf}$ produced by L21A and I60T – 1.3 and 1.1 kcal mol$^{-1}$, respectively – reflect more favorable entropic contributions.

**Table 2**
Conformational stability parameters[a].

| variant | $T_m$ | $\Delta T_m$ | $\Delta H_{vH}$ | $\Delta H_c$ | $\Delta H_{vh}/\Delta H_c$ | $\Delta C_p$ | $\Delta G_{conf}$[b] | *m*-value |
|---|---|---|---|---|---|---|---|---|
| wild-type | 77.3 | – | 52.1 | 61.3 | 0.85 | 0.34 | 6.4 ± 0.3 | 0.83 |
| | (77.0, 77.6) | | (51.0, 52.4) | (60.7, 64.2) | | (0.31, 0.37) | | (0.77, 0.90 |
| M4H | 73.6 | 3.7 | 48.5 | 57.2 | 0.85 | 0.31 | 5.7 ± 0.4 | 0.96 |
| | (73.1, 73.9) | | (48.2, 48.7) | (55.6, 58.0) | | (0.21, 0.42) | | (0.84, 1.09) |
| L21A | 69.1 | 8.2 | 50.9 | 52.2 | 0.98 | 0.58 | 4.8 ± 0.3 | 0.93 |
| | (68.8, 69.4) | | (49.8, 51.7) | (50.9, 54.1) | | (0.45, 0.66) | | (0.83, 1.04) |
| I60T | 70.4 | 6.9 | 53.7 | 63.1 | 0.85 | 0.51 | 5.5 ± 0.4 | 1.03 |
| | (70.2, 70.6) | | (53.5, 54.4) | (62.7, 64.0) | | (0.42, 0.64) | | (0.91, 1.15) |
| C63A | 74.5 | 2.8 | 50.3 | 61.1 | 0.82 | 0.42 | 5.6 ± 0.2 | 0.96 |
| | (74.3, 74.7) | | (49.4, 51.0) | (60.4, 61.8) | | (0.33, 0.50) | | (0.86, 1.07) |
| 21/60 | 61.3 | 16.0 | 49.5 | 55.0 | 0.90 | 0.78 | 3.8 ± 0.2 | 1.05 |
| | (61.1, 61.5) | | (48.8, 50.1) | (54.1, 56.6) | | (0.70, 0.85) | | (0.94, 1.16) |
| 21/60/63 | 57.8 | 19.5 | 45.9 | 56.7 | 0.82 | 0.75 | 3.3 ± 0.2 | 1.14 |
| | (57.6, 58.1) | | (45.2, 46.1) | (56.0, 57.1) | | (0.69, 0.81) | | (1.05, 1.24) |
| 21/60/63/04 | 55.0 | 22.3 | 46.1 | 54.5 | 0.85 | 0.88 | 3.0 ± 0.2 | 1.15 |
| | (54.8, 55.2) | | (45.6, 47.0) | (53.6, 55.8) | | (0.78, 0.95) | | (1.04, 1.26) |

[a] $T_m$ expressed as °C, energies as kcal mol$^{-1}$; $\Delta C_p$ values as kcal mol$^{-1}$ K$^{-1}$, and the *m*-values as kcal mol$^{-1}$ M$^{-1}$. Numbers in parentheses represent 95% confidence intervals.
[b] Stability at 25 °C, calculated with the Gibbs–Helmholtz equation.

**Table 3**
Summary of polcalcin conformational stabilities at 25 °C and 77.3 °C[a].

| | 77.3 °C | | | | | | 25 °C | | | | | |
|---|---|---|---|---|---|---|---|---|---|---|---|---|
| | $\Delta G$ | $\Delta\Delta G$ | $\Delta H$ | $\Delta\Delta H$ | $-T\Delta S$ | $-T\Delta\Delta S$ | $\Delta G$ | $\Delta\Delta G$ | $\Delta H$ | $\Delta\Delta H$ | $-T\Delta S$ | $-T\Delta\Delta S$ |
| wt Phl p 7 | 0 | – | 52.1 | – | −52.1 | – | 6.4 | – | 34.3 | – | −27.9 | – |
| M4H | −0.5 | −0.5 | 49.6 | −2.5 | −50.1 | +2.0 | 5.7 | −0.7 | 33.4 | −0.9 | −27.7 | +0.2 |
| L21A | −1.3 | −1.3 | 55.7 | +3.6 | −57.0 | −4.9 | 4.8 | −1.6 | 25.3 | −9.0 | −20.5 | +7.4 |
| I60T | −1.1 | −1.1 | 57.2 | +5.1 | −58.3 | −6.2 | 5.5 | −0.9 | 30.6 | −3.7 | −25.1 | +2.8 |
| C63A | −0.4 | −0.4 | 51.5 | −0.6 | −51.9 | +0.2 | 5.6 | −0.8 | 29.5 | −4.8 | −23.9 | +4.0 |
| 21/60 | −2.7 | −2.7 | 62.0 | +9.9 | −64.7 | −12.6 | 3.8 | −2.6 | 21.2 | −13.1 | −17.4 | +10.5 |
| 21/60/63 | −3.1 | −3.1 | 60.5 | +8.4 | −63.6 | −11.5 | 3.3 | −3.1 | 21.3 | −13.0 | −18.0 | +9.9 |
| 21/60/63/04 | −3.8 | −3.8 | 65.7 | +13.6 | −69.5 | −17.4 | 3.0 | −3.4 | 19.7 | −14.6 | −16.7 | +11.2 |

[a] All values expressed in kcal mol$^{-1}$.

## 3. Discussion

Attendance at the Gibbs Conference has profoundly impacted my research program. It has fostered a more rigorous and quantitative approach to research problems, hopefully reflected in this manuscript. It has also reinforced my bias that structural and functional observations alone, in the absence of relevant thermodynamic data, cannot yield an accurate model for a biological system. For example, the structure of $Ca^{2+}$-free Phl p 7 (were it available) would offer no clue to as to its anomalous stability. An explanation for the unusual behavior emerges only in the detailed analysis of the energetics of the unfolding transition.

The list of Gibbs attendees, past and present, who have influenced my work is long indeed. I particularly wish to acknowledge Gary Ackers, Wayne Bolen, Enrico Di Cera, Vince Hilser, Tim Lohman, George Makhatadze, Kip Murphy, Andy Robertson, Madeline Shea, and John Shriver. The opportunity to contribute to this collection of papers is a decided honor.

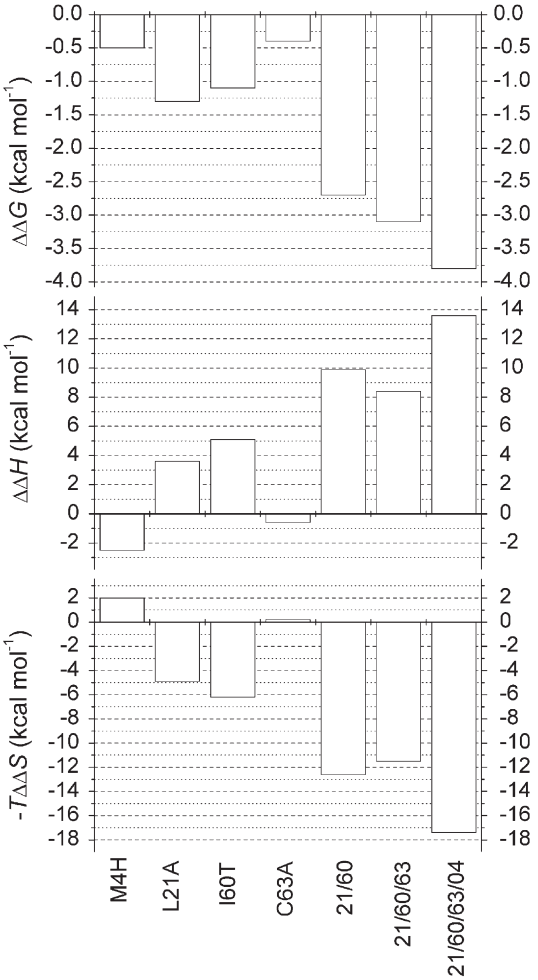


**Fig. 8.** Energetics of unfolding for the Phl p 7 variants, evaluated at 77.3 °C, the wild-type melting temperature.

Phl p 7 exhibits unusually high conformational stability, relative to Bet v 4, Bra n 1, and Bra n 2. This study was undertaken to ascertain whether replacement of select polar side-chains by apolar side-chains might be responsible for the heightened stability of Phl p 7, through an effect on the denatured state ensemble. Thus, the Phl p 7 sequence was inspected for positions at which an apolar side-chain replaced a relatively more polar one in the other three proteins. Four residues satisfying this criterion were identified –– M4, L21, I60, and C63. M4 and L21 reside in EF-hand 1 –– M4 in helix 1 and L21 at the boundary of the binding loop and helix 2. I60 and C63, on the other hand, both reside within EF-hand 2, in helix 4. At each of these positions, the Phl p 7 residue was replaced with the corresponding residue in Bra n 1, the polcalcin having the sequence most closely resembling that of Phl p 7.

The $Ca^{2+}$-binding behavior of each variant protein was examined, to confirm that the mutations did not seriously impact the functionality of the protein. Except for L21A, the variant proteins exhibit perceptibly higher $Ca^{2+}$ affinity than wild-type Phl p 7, with improvements in the overall $\Delta G$ for binding ranging from 0.2 to 0.6 kcal mol$^{-1}$. L21A causes a minor decrease in overall $Ca^{2+}$ affinity ($\Delta\Delta G = +0.1$ kcal mol$^{-1}$). Evidently, it is not uncommon to observe minor functional consequences associated with mutations that significantly perturb conformational stability. For example, although the F7L mutation in barnase destabilizes the protein by 4.6 kcal mol$^{-1}$, the specific activity of the enzyme decreases by just 30% [28].

All four isolated mutations destabilize the protein. At the wild-type $T_m$, the observed $\Delta\Delta G$ values for unfolding, in kcal mol$^{-1}$, are −0.4 (C63A), −0.5 (M4H), −1.1 (I60T), and −1.3 (L21A). M4H and C63A both reduce the enthalpy of unfolding. By contrast, L21A and I60T make unfolding entropically more favorable. The extrapolated changes in stability at 25 °C, in kcal mol$^{-1}$, are −0.7 (M4H), −0.8 (C63A), −0.9 (I60T), and −1.6 (L21A). When the mutations are combined, the resulting protein exhibits a stability comparable to Bra n 1, suggesting that, in fact, the presence of the more apolar residues in Phl p 7 contributes significantly to its heightened stability.

Although the ensuing discussion focuses on the potential impact of the sequence modifications on the denatured state, it is not meant to suggest that there are no effects on the native state. Three of the four mutations (L21A, I60T, C63A) replace a larger side-chain with a smaller one. Although steric effects are not an issue, the resulting elimination of noncovalent interactions significantly destabilizes proteins. In the case of M4H, because the histidyl side-chain geometry differs markedly from that of the linear methionyl side-chain, there is the possibility that the M4H substitution introduces steric interference. M4H does not diminish $Ca^{2+}$-binding affinity, suggesting perhaps that it does not seriously disrupt packing. However, the mutation significantly decreases the enthalpy of unfolding, which could be evidence of a steric clash.

We focus on the unfolded protein because our analysis suggests 1) that the denatured-state ensemble of Phl p 7 is highly compact and 2) that the mutations increase the volume of the DSE. Whereas the random coil was once the accepted model for unfolded proteins, there is now abundant and compelling evidence that the denatured state can retain residual structure, to an extent that is strongly dependent on amino acid sequence [29,30]. Although many denatured proteins are no doubt highly solvated and essentially structureless, others are relatively compact, with restricted solvent accessibility.

The characteristics of the denatured state ensemble (DSE) can be significantly perturbed by single site-specific mutations. Pace and Scholtz have shown that the solvent accessibility of the denatured state increases with net charge, particularly at low pH [31,32]. More relevant to the present work, Pace et al. have recently argued that the extent of unfolding is inversely correlated with the percentage of apolar residues, or mean hydrophobicity [18]. Interestingly, the sequences of intrinsically disordered proteins are distinguished by these same two factors — i.e., high net charge and relatively low mean hydrophobicity [33].

It is well-documented that replacement of bulky, interior side chains with smaller ones can significantly reduce protein stability [28,34,35]. Based on a study of 72 variants, Pace concluded that removal of each completely buried methylene group should destabilize the protein by roughly 1.3 kcal $mol^{-1}$ [36]. He also noted that the magnitude of the effect was consistent with the volume-corrected values of $\Delta G_{tr}$ for transfer of the amino acid side-chains to *n*-octanol.

Although the consequences of the L21A, I60T, and C63A mutations on conformational stability are qualitatively consistent with this idea, the reductions in stability are substantially smaller than predicted. Whereas L21A would be expected to lower Phl p 7 stability by 3.9 kcal $mol^{-1}$, the observed destabilization is just 1.3 kcal $mol^{-1}$. Similarly, the I60T mutation eliminates two methylene groups and should, therefore, lower stability by 2.6 kcal $mol^{-1}$. The observed $\Delta\Delta G$ is just −1.1 kcal $mol^{-1}$. If we consider the thiol group as roughly the equivalent of a methyl group, the C63A mutation effectively eliminates one $-CH_2-$ group and would, therefore, be expected to lower stability by 1.3 kcal $mol^{-1}$. The observed destabilization is 0.4 kcal $mol^{-1}$. Obviously, one possibility for these discrepancies is that the larger side chains are not completely buried in the native wild-type Phl p 7. Alas, structural data for $Ca^{2+}$-free Phl p 7 are lacking. An alternative possibility is that the larger side chains are not completely accessible in the denatured state. In the following paragraphs, we discuss this possibility.

Interestingly, the L21A, I60T, and C63A mutations significantly increase the denaturational heat capacity increment — by 0.08 (C63A), 0.17 (I60T), and 0.24 (L21A) kcal $mol^{-1}$ $K^{-1}$. If the resulting destabilization were solely attributable to solvation, one would predict that the mutations would lower $\Delta C_p$. These unexpected findings merit comment. It should be noted that M4H affords a small reduction in $\Delta C_p$, −0.03 kcal $mol^{-1}$ $K^{-1}$.

It is generally accepted that the $\Delta C_p$ associated with protein conformational transitions primarily reflects the changes in side-chain hydration [37]. Although alternative viewpoints have been advanced [38], the following discussion assumes the general validity of the conventional wisdom. Sturtevant derived the following expression for estimating the hydration-linked component ($\Delta C_{p,\,hyd}$) at 25 °C [39]:

$$\Delta C_{p,\,hyd}(298) = \frac{1.05\Delta C_p - \left(\Delta S^{\circ} - \Delta S_{conf}\right)}{1.31} \tag{6}$$

where $\Delta C_p$ is the observed denaturational heat capacity increment, $\Delta S_u^{\circ}$ is the unfolding entropy corrected to 298 K, and $\Delta S_{conf}$ is the increase in conformational entropy. On a per residue basis, this last value is equal to $R\ln\Delta n$, where $\Delta n$ is the average number of additional conformers populated in the unfolded state. Sturtevant assumed values for $\Delta n$ of 2.2 and 4.8. Having an estimate for $\Delta C_{p,\,hyd}$ at 25 °C, the vibrational contribution to the heat-capacity change at that temperature ($\Delta C_{p,\,vib}$) is then equal to $\Delta C_p - \Delta C_{p,\,hyd}$. Application of this analysis to Bra n 1 and Phl p 7 is illuminating.

Bra n 1, with 78 residues, exhibits a $T_m$ of 331.0 K, a $\Delta C_p$ of 950 cal $mol^{-1}$ $K^{-1}$ (e.u.), and an entropy change on unfolding $\Delta S_u$ at 331 K of 147 e.u. Correcting $\Delta S_u$ to 298 yields $\Delta S_u^{\circ} = 47.2$ e.u. If we assume a $\Delta n$ value of 2.2 – i.e., population, on average, of 2.2 additional conformers in the unfolded state – the calculated conformational entropy change is $1.565 \times 78 = 122$ e.u. (i.e., $R\ln\Delta n$). Substituting these numbers into Eq. (6) yields a value for $\Delta C_{p,\,hyd}(298)$ of 818 e.u. and a corresponding $\Delta C_{p,\,\underline{vib}}$ of 132 e.u.

Phl p 7, with 77 residues, exhibits a $T_m$ of 350.4 K, $\Delta C_p$ of 340 cal $mol^{-1}$ $K^{-1}$, an entropy change on unfolding at that temperature, $\Delta S_u(350.4)$, of 149 cal $mol^{-1}$ $K^{-1}$, and a conformational entropy change (again assuming an additional 2.2 conformers per residue) of $1.565 \times 78 = 120.5$ cal $mol^{-1}$ $K^{-1}$. Substituting these numbers into Eq. (6) yields a value for $\Delta C_{p,\,hyd}(298)$ of 293 cal $mol^{-1}$ $K^{-1}$ and a corresponding $\Delta C_{p,\,\underline{vib}}$ of 47 e.u.

These calculations strongly suggest that, their general sequence similarity notwithstanding, the unfolded states of Bra n 1 and Phl p 7 differ profoundly. Solvent accessibility is evidently markedly depressed in the latter, and there is a much lower vibrational entropy. These observations suggest that the thermally denatured state of Phl p 7 may more closely resemble a molten globule than a random coil. In this context, thermal denaturation of $Ca^{2+}$-bound α-lactalbumin is believed to yield a molten-globule state [40].

The assumption of a compact denatured state for Phl p 7 provides a rationale for the increase in $\Delta C_p$ that accompanies the L21A, I60T, and C63A mutations. A priori, replacement of an apolar side-chain with relatively more polar ones should lower the heat capacity change that accompanies unfolding, if the increase in heat-capacity results primarily from the ordering of water around solvent-exposed hydrophobic groups. Of course, this line of reasoning is predicated on the notion that the unfolded state resembles a random coil — i.e., the side-chains have unfettered rotational mobility and are completely solvent accessible. If, in fact, the wild-type denatured state is compact, with restricted solvent access, then these mutations, by eliminating a more bulky hydrophobic group, might paradoxically increase the ΔASA by encouraging expansion of the DSE, resulting in greater solvent accessibility and increased conformational entropy. In this context, Fu et al. [41] report that the D79F mutation in RNaseA, which increases stability by a whopping 7.7 kcal $mol^{-1}$, is accompanied by a paradoxical 0.6 kcal $mol^{-1}$ $K^{-1}$ decrease in $\Delta C_p$. The authors similarly attribute the effect to increased residual structure in the unfolded state.

Denaturant *m* values, like $\Delta C_p$ values, are also proportional to the change in accessible surface area on unfolding [42]. The changes in the *m* value resulting from the four polcalcin mutations described here are also larger than one would predict based merely on changes in solvation. Auton et al. [43] have argued convincingly that the destabilizing action of urea is almost exclusively a consequence of favorable interaction with the polypeptide backbone [43]. In their paper, they present the following equation for predicting the urea *m* value:

$$m_{\mathrm{calc}} = \sum_{i=\mathrm{AA\ type}}^{\mathrm{sidechains}} n_i \cdot GTFE_i^{*} \cdot \Delta\alpha_i^{sc} + GTFE^{bb} \cdot \sum_{i=\mathrm{AA\ type}}^{\mathrm{backbone}} n_i \cdot \Delta\alpha_i^{bb}. \tag{9}$$

In this equation, $n_i$ is the number of residues of type *i*.$GTFE^{bb}$ is the group transfer free energy for the backbone moiety of an amino acid residue, and $GTFE_i^{*}$ is the corrected group transfer free energy for the side-chain of amino acid type *i* — i.e., incorporating an improved estimate for the *GTFE* of the glycyl residue. Auton et al. [43] provide $GTFE_i^{*}$ values for nearly all of the amino acids. The symbols $\Delta\alpha_i^{sc}$ and

$\Delta\alpha_i^{bb}$ represent the fractional change in solvent accessibility upon unfolding for the side chain and backbone moieties of residue type *i*.

Evaluation of $\Delta\alpha_i^{sc}$ and $\Delta\alpha_i^{bb}$ requires structural data for the protein of interest, so that the accessibility in the native state can be estimated. Although structural data for Phl p 7 are lacking, we can nevertheless predict the change in *m* resulting from a given mutation if the impact was solely due to differential solvation. For example, if Eq. (9) for wild-type Phl p 7 is subtracted from the corresponding equation for the L21A variant, all of the terms disappear except the side-chain contributions for residue 21, yielding

$$\Delta m_{calc} = GTFE^*_{Ala} * \Delta\alpha^{sc}_{Ala} - GTFE^*_{Leu} * \Delta\alpha^{sc}_{Leu} = 0.63\Delta\alpha^{sc}_{Ala} - (-14.30)\Delta\alpha^{sc}_{Leu} \quad (10)$$

Whereas our analysis indicates that the replacement of L21 by alanine raises *m* from 830 to 930 cal mol$^{-1}$ M$^{-1}$, the maximal predicted increase in *m* is just 15 cal mol$^{-1}$ M$^{-1}$ — based on a maximal fractional change in accessibility of 1.0 for both residues. For the I60T substitution, the discrepancy is even larger. The experimental change in *m* is 200 cal mol$^{-1}$ M$^{-1}$. The maximal predicted change is 16.4 cal mol M$^{-1}$, according to the following calculation:

$$\Delta m_{calc} = GTFE^*_{Thr} * \Delta\alpha^{sc}_{Thr} - GTFE^*_{Ile} * \Delta\alpha^{sc}_{Ile} = 18.2\Delta\alpha^{sc}_{Thr} - (1.84)\Delta\alpha^{sc}_{Ile} \quad (11)$$

A large discrepancy in the measured and predicted $\Delta m_{calc}$ values is likewise observed for M4H, +130 and −2 cal mol$^{-1}$ M$^{-1}$, respectively. The absence of a $GTFE_i$* value for cysteine precludes a similar analysis for the C63A mutation.

Like the $\Delta\Delta C_p$ values, the $\Delta m$ values are likewise consistent with the notion that increased apolar content produces a more compact denatured state ensemble (DSE). Thus, elimination of the hydrophobic side-chains would yield an expanded DSE with higher configurational entropy and consequently lower native-state stability. Introduction of either L21A or I60T causes unfolding to become entropically more favorable. The resulting DSE would also experience increased solvent accessibility, leading to more effective solvation of the remaining apolar side-chains and consequently greater $\Delta C_p$.

The observed changes in stability are largely, but not entirely, additive. Evaluated at the wild-type $T_m$ (77.3 °C), the $\Delta\Delta G$ values for the four isolated mutations sum to −3.3 kcal mol$^{-1}$. However, the $\Delta\Delta G$ value measured for the 21/60/63/04 variant is −3.8 kcal mol$^{-1}$. Of this 0.5 kcal mol$^{-1}$ discrepancy, 0.3 kcal mol$^{-1}$ is attributable to the interaction between the L21A and I60T substitutions. The isolated mutations alter conformational stability by −1.3 and −1.1 kcal mol$^{-1}$, respectively. Combined, they lower stability by 2.7 kcal mol$^{-1}$. The remaining 0.2 kcal mol$^{-1}$ is assignable to M4H. Alone, the mutation yields a $\Delta\Delta G$ of −0.5 kcal mol$^{-1}$. When introduced into 21/60/63, the M4H substitution reduces stability by 0.7 kcal mol$^{-1}$. These observations suggest that the consequences of the mutations are not independent, consistent perhaps with the retention of residual structure in the denatured state of Phl p 7. There is precedence for this behavior in staphylococcal nuclease [30,44]. As observed here, the magnitudes of the cooperative effects in SNase are not large, but nevertheless significant.

Although the structure of $Ca^{2+}$-free Phl p 7 is not available, the solution structure of $Ca^{2+}$-bound Bet v 4 has been solved, as noted previously. The residues in Bet v 4 corresponding to M4, L21, and I60 are R11, A28, and T67. In the Bet v 4 solution structure, the side-chains of R11 and A28 are in van der Waals contact. Although well-separated in the $Ca^{2+}$-loaded structure, A28 and T67 could actually be in closer proximity in the apo-protein, given that the polcalcin tertiary structure undergoes a major conformational change upon $Ca^{2+}$ binding. However, proximity in the native state is evidently not required, as the data of Green and Shortle [44] suggest that interactions between residues in the DSE can extend beyond 20 Å.

## 4. Conclusions

The data presented here suggest that the atypical conformational stability of Phl p 7 is achieved via substitution of apolar amino acids at strategic positions in the polypeptide chain. When M4, L21, I60, and C63 are replaced by the corresponding residues in the Bra n 1 sequence, the stability of the resulting protein approaches that of Bra n 1. It may be noted that all of the mutations have a modest influence on $Ca^{2+}$ affinity. Our analysis of the M4H, I60T, C63A, and L21A mutations suggests that their impact is primarily on the denatured state. First, the diminutive denaturational heat capacity increment displayed by wild-type Phl p 7 indicates a relatively structured unfolded state. Secondly, the thermodynamic consequences of the mutations are unusual. Consider L21A, for example. The mutation provokes a fairly modest decrease in conformational stability; it paradoxically increases the $\Delta C_p$ associated with denaturation; and it substantially raises the urea *m* value. All three observations would be consistent with a decrease in residual structure in the unfolded state. Similar arguments can be advanced for the I60T and C63A mutations. The M4H mutation is somewhat different, because the change in side-chain geometry could also introduce a steric conflict. Although M4H does not increase the denaturational heat capacity increment ($\Delta\Delta C_p = -0.03$ kcal mol$^{-1}$ K$^{-1}$), the increase in urea *m* value eclipses the increases observed for the other three mutations. Finally, the energetic consequences of the mutations are apparently non-additive. The impact of L21A is more pronounced in the presence of I60T, and vice-versa. Similarly, M4H has a greater destabilizing effect in the presence of the other three mutations. Future studies will seek to more fully characterize the denatured state of Phl p 7. It would be of interest, for example, to compare the hydrodynamic behaviors of urea-denatured Phl p 7 and Bra n 1. Specifically, is the ratio of the observed frictional coefficient to that calculated for the unhydrated spherical protein – i.e., $f/f^\circ$ – perceptibly smaller for Phl p 7? We also plan to compare the $^1$H,$^{15}$N-HSQC spectra of urea-denatured Phl p 7 and Bra n 1 — anticipating that the Phl p 7 spectrum will exhibit greater dispersion, indicative of residual ordered structure.

## Acknowledgment

The author (M.T.H) gratefully acknowledges support from NSF (MCB0543476) and the University of Missouri Research Board.

## References

[1] E. Engel, K. Richter, G. Obermeyer, P. Briza, A.J. Kungl, B. Simon, M. Auer, C. Ebner, H.J. Rheinberger, M. Breitenbach, F. Ferreira, Immunological and biological properties of Bet v 4, a novel birch pollen allergen with two EF-hand calcium-binding domains, J. Biol. Chem. 272 (1997) 28630–28637.
[2] A. Ledesma, M. Villalba, E. Batanero, R. Rodriguez, Molecular cloning and expression of active Ole e 3, a major allergen from olive-tree pollen and member of a novel family of $Ca^{2+}$-binding proteins (polcalcins) involved in allergy, Eur. J. Biochem. 258 (1998) 454–459.
[3] K. Rozwadowski, R. Zhao, L. Jackman, T. Huebert, W.E. Burkhart, S.M. Hemmingsen, J. Greenwood, S.J. Rothstein, Characterization and immunolocalization of a cytosolic calcium-binding protein from *Brassica napus* and *Arabidopsis* pollen, Plant Physiol. 120 (1999) 787–798.
[4] C. Suphioglu, F. Ferreira, R.B. Knox, Molecular cloning and immunological characterization of Cyn d 7, a novel calcium-binding allergen from Bermuda grass pollen, FEBS Lett. 402 (1997) 167–172.
[5] T. Okada, Z. Zhang, S.D. Russell, K. Toriyama, Localization of the $Ca^{2+}$-binding protein, Bra r 1, in anthers and pollen tubes, Plant Cell Physiol. 40 (1999) 1243–1252.
[6] B. Hayek, L. Vangelista, A. Pastore, W.R. Sperr, P. Valent, S. Vrtala, V. Niederberger, A. Twardosz, D. Kraft, R. Valenta, Molecular and immunologic characterization of a highly cross-reactive two EF-hand calcium-binding alder pollen allergen, Aln g 4: structural basis for calcium-modulated IgE recognition, J. Immunol. 161 (1998) 7031–7039.
[7] V. Niederberger, B. Hayek, S. Vrtala, S. Laffer, A. Twardosz, L. Vangelista, W.R. Sperr, P. Valent, H. Rumpold, D. Kraft, K. Ehrenberger, R. Valenta, S. Spitzauer,

Calcium-dependent immunoglobulin E recognition of the apo- and calcium-bound form of a cross-reactive two EF-hand timothy grass pollen allergen, Phl p 7, FASEB J. 13 (1999) 843–856.
[8] M.T. Henzl, M.E. Davis, A. Tan, Divalent ion binding properties of the timothy grass allergen, Phl p 7, Biochemistry 47 (2008) 7846–7856.
[9] M.T. Henzl, M.E. Davis, A. Tan, Polcalcin divalent ion-binding behavior and thermal stability: comparison of Bet v 4, Bra n 1, and Bra n 2 to Phl p 7, Biochemistry 49 (2010) 2256–2268.
[10] A. Twardosz, B. Hayek, S. Seiberler, L. Vangelista, L. Elfman, H. Gronlund, D. Kraft, R. Valenta, Molecular characterization, expression in *Escherichia coli*, and epitope analysis of a two EF-hand calcium-binding birch pollen allergen, Bet v 4, Biochem. Biophys. Res. Commun. 239 (1997) 197–204.
[11] P. Neudecker, J. Nerkamp, A. Eisenmann, A. Nourse, T. Lauber, K. Schweimer, K. Lehmann, S. Schwarzinger, F. Ferreira, P. Rosch, Solution structure, dynamics, and hydrodynamics of the calcium-bound cross-reactive birch pollen allergen Bet v 4 reveal a canonical monomeric two EF-hand assembly with a regulatory function, J. Mol. Biol. 336 (2004) 1141–1157.
[12] P. Verdino, K. Westritschnig, R. Valenta, W. Keller, The cross-reactive calcium-binding pollen allergen, Phl p 7, reveals a novel dimer assembly, EMBO J. 21 (2002) 5007–5016.
[13] M.R. Celio, T. Pauls, B. Schwaller, Guidebook to the Calcium-binding Proteins, Oxford University Press, New York, 1996.
[14] R.H. Kretsinger, Structure and evolution of calcium-modulated proteins, CRC Crit. Rev. Biochem. 8 (1980) 119–174.
[15] H. Kawasaki, R.H. Kretsinger, Calcium-binding proteins 1: EF-hands, Protein Profile 2 (1995) 297–490.
[16] R.H. Kretsinger, C.E. Nockolds, Carp muscle calcium-binding protein. II. Structure determination and general description, J. Biol. Chem. 248 (1973) 3313–3326.
[17] C.A. McPhalen, N.C.J. Strynadka, M.N.G. James, Calcium-binding sites in proteins: a structural perspective, Adv. Protein Chem. 42 (1991) 77–144.
[18] C.N. Pace, B.M.P. Huyghues-Despointes, H. Fu, K. Takano, J.M. Scholtz, G.R. Grimsley, Urea denatured state ensembles contain extensive secondary structure that is increased in hydrophobic proteins, Protein Sci. 19 (2010) 929–943.
[19] M. Haner, M.T. Henzl, B. Raissouni, E.R. Birnbaum, Synthesis of a new chelating gel: removal of $Ca^{2+}$ ions from parvalbumin, Anal. Biochem. 138 (1984) 229–234.
[20] M.T. Henzl, S. Agah, J.D. Larson, Characterization of the metal ion-binding domains from rat α- and β-parvalbumins, Biochemistry 42 (2003) 3594–3607.
[21] M.T. Henzl, J.D. Larson, S. Agah, Estimation of parvalbumin $Ca^{2+}$- and $Mg^{2+}$-binding constants by global least-squares analysis of isothermal titration calorimetry data, Anal. Biochem. 319 (2003) 216–233.
[22] M.T. Henzl, Characterization of parvalbumin and polcalcin divalent ion binding by isothermal titration calorimetry, Methods Enzymol. 455 (2009) 259–296.
[23] J.R. Warren, J.A. Gordon, On the refractive indices of aqueous solutions of urea, J. Phys. Chem. 70 (1996) 297–300.
[24] D.T. Haynie, Quantitative analysis of differential scanning calorimetric data, in: J.E. Ladbury, B.Z. Chowdhry (Eds.), Biocalorimetry. Applications of Calorimetry in the Biological Sciences, John Wiley & Sons, New York, 1998, pp. 183–205.
[25] C.N. Pace, D.V. Laurents, A new method for determining the heat capacity change for protein folding, Biochemistry 28 (1989) 2520–2525.
[26] B.S. McCrary, S.P. Edmondson, J.W. Shriver, Hyperthermophile protein folding thermodynamics: differential scanning calorimetry and chemical denaturation of Sac7d, J. Mol. Biol. 264 (1996) 784–805.
[27] M.M. Santoro, D.W. Bolen, Unfolding free energy changes determined by the linear extrapolation method. 1. Unfolding of phenylmethanesulfonyl α-chymotrypsin using different denaturants, Biochemistry 27 (1988) 8063–8068.
[28] J.T. Kellis Jr., K. Nyberg, D. Sali, A.R. Fersht, Contributions of hydrophobic interactions to protein stability, Nature 333 (1988) 784–786.
[29] D. Shortle, Staphylococcal nuclease: a showcase of m-value effects, Adv. Protein Chem. 46 (1995) 217–247.
[30] D. Shortle, The denatured state (the other half of the folding equation) and its role in protein stability, FASEB J. 10 (1996) 27–34.
[31] C.N. Pace, K.L. Shaw, Linear extrapolation method of analyzing solvent denaturation curves, Proteins 41 (2000) 1–7.
[32] C.N. Pace, R.W. Alston, K.L. Shaw, Charge–charge interactions influence the denatured state ensemble and contribute to protein stability, Protein Sci. 9 (2000) 1395–1398.
[33] V.N. Uversky, J.R. Gillespie, A.L. Fink, Why are "natively unfolded" proteins unstructured under physiologic conditions? Proteins 41 (2000) 415–427.
[34] J.T. Kellis Jr., K. Nyberg, A.R. Fersht, Energetics of complementary side-chain packing in a protein hydrophobic core, Biochemistry 28 (1989) 4914–4922.
[35] D. Shortle, W.E. Stites, A.K. Meeker, Contributions of the large hydrophobic amino acids to the stability of staphylococcal nuclease, Biochemistry 29 (1990) 8033–8041.
[36] C.N. Pace, Contribution of the hydrophobic effect to globular protein stability, J. Mol. Biol. 226 (1992) 29–35.
[37] R.S. Spolar, J.R. Livingstone, M.T. Record, Use of liquid hydrocarbon and amide transfer data to estimate contributions to thermodynamic functions of protein folding from the removal of nonpolar and polar surface from water, Biochemistry 31 (1992) 3947–3955.
[38] A. Cooper, Heat capacity effects in protein folding and ligand binding: a re-evaluation of the role of water in biomolecular thermodynamics, Biophys. Chem. 115 (2005) 89–97.
[39] J.M. Sturtevant, Heat capacity and entropy changes in processes involving proteins, Proc. Natl. Acad. Sci. U.S.A. 74 (1977) 2236–2240.
[40] G. Vanderheeren, I. Hanssens, Thermal unfolding of bovine α-lactalbumin, J. Biol. Chem. 269 (1994) 7090–7094.
[41] H. Fu, G. Grimsley, J.M. Scholtz, C.N. Pace, Increasing protein stability: importance of $\Delta C_p$ and the denatured state, Protein Sci. 19 (2010) 1044–1052.
[42] J.K. Myers, C.N. Pace, J.M. Scholtz, Denaturant m values and heat capacity changes: relation to changes in accessible surface areas of protein unfolding, Protein Sci. 4 (1995) 2138–2148.
[43] M. Auton, L.M.F. Holthauzen, D.W. Bolen, Anatomy of energetic changes accompanying urea-induced protein denaturation, Proc. Natl. Acad. Sci. U.S.A. 104 (2007) 15317–15322.
[44] S.M. Green, D. Shortle, Patterns of nonadditivity between pairs of stability mutations in staphylococcal nuclease, Biochemistry 32 (1993) 10131–10139.